ADVANCED THERAPEUTICS
www.advtherap.com

Lysine-Derived Carbon Dots for Chiral Inhibition of Prion Peptide Fibril Assembly

*Elad Arad, Susanta Kumar Bhunia, Jürgen Jopp, Sofiya Kolusheva, Hanna Rapaport, and Raz Jelinek**

The transmissible spongiform encephalopathies are a family of diseases characterized by abnormal folding and aggregation of the prion protein. One of the directions in the search for cure for these and other amyloid diseases focuses on the inhibition of protein aggregation by small molecules, short peptides, and nanoparticles. Nanoparticles seem to be particularly promising therapeutic candidates since they are stable, can be made biocompatible, and might readily traverse physiological barriers such as the blood–brain barrier. Here, a novel class of chiral amyloid inhibitors consisting of carbon quantum dots (C-dots) that are synthesized from either D- or L-lysine (Lys) as the sole carbonaceous building block are reported. The interactions of the chiral lys-C-dots with the amyloidogenic determinant of the prion peptide (PrP, 106–126 sequence) in the presence of lipid bilayers appears to be highly stereoselective, with the L-Lys-C-dots being superior to the D-Lys-C-dots in their ability to modulate the structural transformations and aggregation of PrP(106–126). This work provides new insights into chiral effects upon amyloid peptides and opens the way to developing chiral carbon-based nanostructures as advanced amyloid inhibitors.

1. Introduction

Amyloidosis is a term used to describe a group of human and animal diseases in which a functioning protein is misfolded into insoluble fibrils. Amyloid fibrils are deposited in the extracellular spaces of organs and tissues, leading to the formation of plaques and disrupting the organ's function. The chronic neuronal and systemic pathologies caused by these aggregates are associated with a wide range of often fatal neurodegenerative diseases,[1] including Alzheimer's disease, transmissible spongiform encephalopathies (TSEs), type II diabetes, and others.[2–4] Although the exact mechanisms of fibril formation are not known, it has been proposed that the process takes place in two phases: a lag phase in which the native globular form of the protein is lost and a β-sheet structure is developed, and an elongation phase in which the β-sheet intermediates are converted into soluble oligomers, protofibrils, and insoluble fibrils that ultimately aggregate to form the fibrillar plaques.[5,6]

TSE is a devastating protein misfolding disease afflicting animals and humans. There is no therapy available for the diverse group of prion diseases, which include Creutzfeldt–Jakob disease and Gerstmann–Sträussler–Scheinker disease in humans, bovine spongiform encephalopathy in cattle, scrapie in sheep, and chronic wasting disease in cervids.[7–9] The *prion hypothesis* accounts for the spread and pathogenicity of TSE.[10] Specifically, the conversion of the normal cellular form of the prion peptide, PrP^{C}, to the infectious form PrP^{Sc} is theorized to be a causative agent affecting the brains of people and animals suffering from these diseases.[11–14] This abnormality is manifested as a conformation change of the protein from an α-helix into a β-sheet; this transformation has apparent catalytic properties, propagating within the surrounding proteins. The 21-residue 106–126 fragment of PrP (i.e., PrP(106–126)) has been shown to constitute the amyloidogenic determinant of the prion protein, and numerous studies have focused on this peptide for fibrillation and toxicity studies.[15,16] Importantly, membranes have been shown to play insidious and prominent roles in fibrillation of PrP fragments.[17–19]

Varied substances have been tested for their ability to prevent/retard amyloid plaque formation, including small molecules (primarily polyphenols),[20–22] peptides,[23] polymers,[12,24] and nanoparticles.[25,26] In the search for effective inhibitor compounds, a variety of aggregate features have been targeted. For example, mechanistic considerations have led to the targeting of the forces stabilizing the aggregates by introducing competing hydrogen bonds, using detergent-like compounds to interrupt hydrophobic and electrostatic interactions.[27,28] Other types of inhibitor have been designed to interfere with π-stacking and fibril elongation.[29,30] Yet another strategy targets

E. Arad, Dr. S. K. Bhunia, Prof. R. Jelinek
Department of Chemistry
Ben Gurion University of the Negev
Beer Sheva 84105, Israel
E-mail: razj@bgu.ac.il
J. Jopp, Dr. S. Kolusheva
Ilse Katz Institute (IKI) for Nanoscale Science and Technology
Ben Gurion University of the Negev
Beer Sheva 84105, Israel
Prof. H. Rapaport
Avram and Stella Goldstein–Goren Department of Biotechnology Engineering and Ilse Katz Institute (IKI) for Nanoscale Science and Technology
Ben Gurion University of the Negev
Beer Sheva 84105, Israel

DOI: 10.1002/adtp.201800006

the fibrillar β-sheet *chiral* arrangement; while changing the chirality of one of the strands, the ability of the β-strands to organize one next to the other is diminished.[31–33]

Carbon quantum dots (C-dots) are unique carbonaceous nanoparticles, attracting significant interest because of their small size (<10 nm), tunable fluorescence emission properties,[34] available surface functionalization routes, low toxicity, and biocompatibility.[35] C-dots have been employed in diverse applications, including bioimaging,[36,37] chemical and biological sensing,[38] catalysis,[39] and photo-induced electron transfer properties.[40–47] In general, C-dots exhibit crystalline graphite cores surrounded by shells of different organic groups. Recent studies demonstrated intriguing therapeutic applications of C-dots. In the context of amyloid diseases, Leblanc and colleagues, inspired by β-sheet-targeting peptides, exploited C-dots to inhibit aggregation of insulin peptides. They and others have also suggested that biomimetic C-dots, which are capable of crossing the blood–brain barrier, can be applied for in vivo inhibition of amyloid plaques in brain tissue.[48,49]

Here, we report synthesis of *chiral* C-dots from either L-lysine or D-lysine as the sole carbonaceous building blocks and their use as fibrillation modulators for PrP(106–126). Poly-L-lysine (PLL) chains have been shown to inhibit PrP propagation in vitro and in vivo.[24] While chiral C-dots have been recently reported,[50] they were produced by coupling of chiral residues to synthesized (non-chiral) C-dots. The study presented here, however, constitutes, to the best of our knowledge, the first demonstration of endowing C-dot chirality through direct hydrothermal synthesis utilizing enantiomeric building blocks (L-Lys or D-Lys). Indeed, recent studies have demonstrated that C-dots retain "structural memory" of the carbon-containing compounds employed as building blocks.[39,51,52] We show that L-Lys-C-dots exert significant effects, different than D-Lys-C-dots, upon PrP(106–126) structural features and fibrillation kinetics in the presence of biomimetic lipid bilayers. The dramatic chiral effects might open new avenues for both elucidating the aggregation process of the prion protein, as well as for development of new therapeutic routes against amyloid diseases using carbon dots.

2. Results

2.1. C-dot Synthesis and Characterization

C-dots were prepared from either L-Lys or D-Lys enantiomers as the only carbonaceous building block, designed to endow opposite chirality to the carbon nanoparticles. Importantly, synthesis conditions (i.e., temperature and duration of hydrothermal treatment) for both L-Lys-C-dots and D-Lys-C-dots were the same, designed to ascertain that the two C-dot species would exhibit similar physical properties (such as size distribution, graphitic core structure, surface functionalities), and the only difference being their overall chirality. Circular dichroism (CD) spectra of the L-Lys-C-dots and D-Lys-C-dots in **Figure 1** confirm that the opposite chirality of the amino acid enantiomers was retained in the synthesized C-dots. Specifically, the CD signatures of Lys-C-dots show a mirror-image ellipticity, with a *minimum* for the D-enantiomer at 210–220 nm and a *maximum* for the L-enantiomer at the same wavelength range. The CD data in Figure 1 indicate that the lysine moieties on the C-dots surface display only one enantiomer. Previous reports similarly showed that carbon-based nanoparticles coated with enantiomeric molecules produced CD spectra displaying a positive maximum for the L-enantiomer and negative minimum for the D-enantiomer.[50,53]

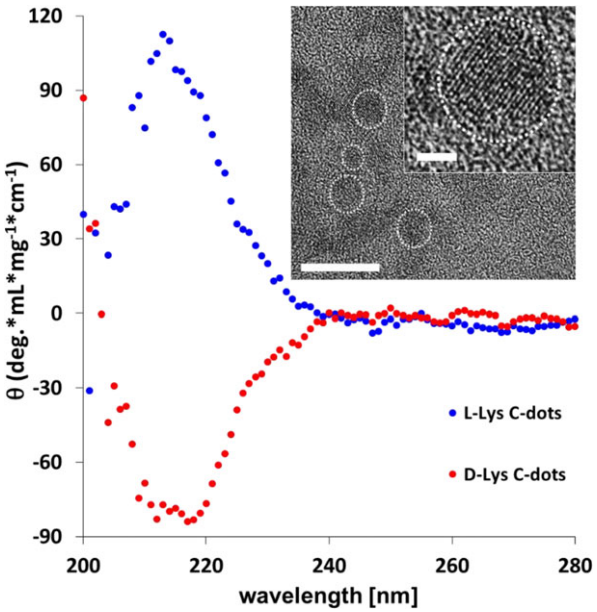

Figure 1. Spectroscopic and microscopic characterization of lysine-derived C-dots. Opposite ellipticities of 3.0 mg mL^{-1} L-Lys-C-dots (blue) and D-Lys-C-dots (red). Spectra were normalized according to C-dots concentration and cuvette length. Inset: high-resolution transmission electron microscopy images of L-Lys-C-dots. The scale bar corresponds to 10 nm. The magnified image shows the [110] crystalline graphitic lattice planes within the C-dot core; scale bar corresponds to 2 nm.

The high-resolution transmission electron microscopy (HR-TEM) images in the inset of Figure 1 underscore the relatively uniform size distribution of the C-dots (statistical analysis based upon the TEM data indicate C-dot diameters of 4 ± 1.2 nm, $n = 50$, Figure S1, Supporting Information), and confirm the crystallinity of the C-dots' graphitic cores. The magnified HR-TEM image in the inset of Figure 1 reveals the crystal planes exhibiting lattice spacing of 0.215 nm, corresponding to the [110] planes of graphite.[46,51,54] Importantly, while the microscopy data in Figure 1 correspond to L-Lys-C-dots, similar images were recorded in case of D-Lys-C-dots. Excitation-dependent fluorescence emission spectra (Figure S2, Supporting Information), UV-Vis absorbance spectra (Figure S3, Supporting Information), and X-ray photoelectron spectroscopy experiments (XPS, Figures S4 and S5, Supporting Information) confirm that the L-Lys-C-dots and D-Lys-C-dots exhibit highly similar physical properties. Fourier transform IR (FTIR) spectroscopy data in Figure S6, Supporting Information reveal chemically similar and typical lysine functional groups on both C-dots' surfaces.

2.2. Aggregation of PrP(106–126) in the Presence of Chiral C-Dots

Aggregation of PrP(106–126) was studied in solutions containing each of the Lys-C-dot enantiomers, in order to track their effect

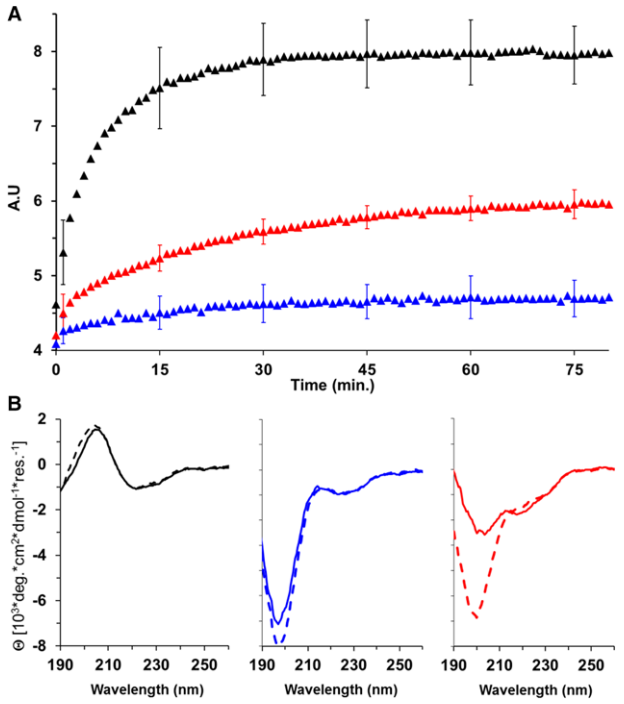

Figure 2. Effects of C-dots upon PrP(106–126) structures and aggregation. A) ThT fluorescence kinetics (ThT 10 μM, PrP 50 μM, DMPC:DMPG lipid vesicles 0.2 mM, Lys-C-dots 0.1 mg mL^{-1}). Data presented as mean ± SD, $n = 4$, three replicates each. B) Secondary structure analysis using CD spectroscopy of PrP in DMPC/DMPG vesicle solutions (1:1 mole ratio). Broken spectra: immediately after dissolution; solid spectra: 15 min after dissolution. In A and B: *black spectra* represent PrP(106–126) alone in the vesicle solution, *blue spectra* represent PrP(106–126) in the presence of L-Lys-C-dots, and *red spectra* represent PrP(106–126) in the presence of D-Lys-C-dots. Spectra were normalized according to the number of residues, cuvette length, and concentration.

on aggregation kinetics, structure, and morphology of the prion fibrils. Since PrP(106–126) fibrillation occurs in biomimetic membrane environments, the experiments summarized in **Figures 2–4** were carried out in aqueous solutions containing dimyristoyl-sn-glycero-3-phosphocholine (DMPC)/1,2-ditetradecanoyl-sn-glycero-3-phospho-(1′-rac-glycerol) (DMPG) lipid bilayers. Figure 2A depicts the aggregation kinetics of PrP in a DMPC:DMPG vesicle solution (1:1 mole ratio), in the presence of L-Lys-C-dots or D-Lys-C-dots, by using the thioflavin-T (ThT) fluorescence assay, which is widely used for the assessment of amyloid fibril assembly. The fluorescence emission of ThT, a benzothiazole derivative, increases in the presence of amyloid aggregates.[3,4] Importantly, the fluorescence emission shown in Figure 2A accounts only to ThT increase due to PrP aggregation, as the fluorescence emission of all components present in the solution (e.g., vesicles, C-dots) was subtracted. The control ThT curve (no C-dots added to PrP(106–126)) showed enhanced fluorescence approximately after 15 min, which remained stable for the remainder of the measurement period. However, the ThT curves in Figure 2A demonstrate that both D-Lys-C-dots and particularly L-Lys-C-dots significantly reduced ThT fluorescence, likely impairing the formation of β-sheet structures within PrP(106–126) aggregates.

In light of the ThT results in Figure 2 suggesting that the C-dots interfere in the fibrillation process, we sought to investigate in greater depth the effect of the chiral Lys-C-dots on the solution conformations of PrP(106–126), particularly β-sheet assembly. To this end, the structural transformations of PrP(106–126), in the absence and presence of the L- or D-enantiomer of Lys-C-dots, were followed by CD spectroscopy. PrP(106–126) alone instantaneously adopted a β-sheet conformation, giving rise to a maximum at 205 nm and minimum at 220 nm, upon dissolution in an aqueous vesicle solution (Figure 2B, black spectra).[[15] Notably, the low CD spectral intensity of PrP(106–126) without the presence of C-dots likely reflects rapid aggregation of the peptide.

In comparison, samples containing PrP(106–126) and the two chiral Lys-C-dots both exhibited a deep minimum at 198 nm immediately after dissolution, corresponding to a random coil unfolded structure (Figure 2B, blue and red broken spectra, respectively). After 15 min, no significant change was apparent in the CD spectrum of PrP(106–126) in the presence of L-Lys-C-dots (Figure 2B, blue solid spectrum), indicating inhibition of β-sheet assembly. The 15-min CD spectrum of PrP(106–126) in the presence of D-Lys-C-dots featured two minima, at 200 nm and 220 nm (Figure 2B, blue solid spectrum), indicating both random coil and β-sheet structures of the peptide. Overall, the CD data in Figure 2B (blue and red spectra) provide evidence that the C-dots interfered with adoption of β-sheet assembly by PrP(106–126), corroborating the ThT fluorescence results which pointed to slower aggregation kinetics of the peptide induced by the carbon nanoparticles.

Figure 3 presents microscopy analyses demonstrating dramatic enantiomer-dependent effects of the C-dots upon PrP(106–126) fibril morphologies. The atomic force microscopy (AFM) images in Figure 3A–C, recorded following incubation of the peptide upon a silicon substrate coated with a DMPC/DMPG bilayer (1:1 mole ratio), reveal significant differences in PrP(106–126) fibril shapes, lengths, and relative abundance, among the samples examined. Specifically, in the absence of C-dots, PrP(106–126) produced major fibril aggregates, manifested in the AFM image as a dense plaque made up of entangled fibers (Figure 3A). In contrast, very low fibril content was observed upon co-incubation of PrP(106–126) with L-Lys-C-dots (Figure 3B). Moreover, the PrP(106–126) fibrils appeared much shorter and not twisted—a significantly different result as compared to the native peptide aggregates without addition of C-dots, that is, Figure 3A. Greater abundance of PrP(106–126) fibers was apparent when PrP(106–126) was pre-incubated with D-Lys-C-dots (Figure 3C). However, the PrP(106–126)/D-Lys-C-dot sample gave rise to thinner fibrils that did not display the entangled morphology observed in case of the untreated, native peptide (i.e., Figure 3A).

The cryogenic transmission electron microscopy (cryo-TEM) images in Figure 3D–F, displaying PrP(106–126) fibrils incubated in a DMPC:DMPG vesicle solution together with D-Lys-C-dots or L-Lys-C-dots, were consistent with the AFM analysis. Specifically, PrP(106–126) that was not treated with C-dots gave rise to dense fibril domains spread on the TEM grid (Figure 3D). However, a much lower concentration of shorter fibrils was recorded in case of PrP(106–126) incubated with L-Lys-C-dots (Figure 3E). D-Lys-C-dots did not induce such a significant PrP(106–126) fibril inhibition (Figure 3F), however, similar to the AFM result in Figure 3C, a lower fibril content was apparent in

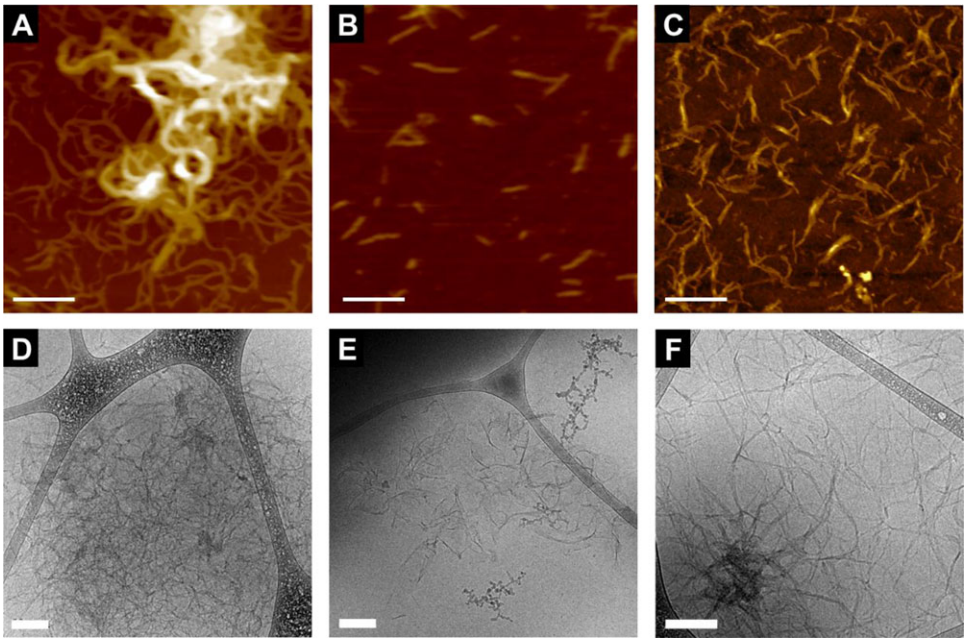

Figure 3. Morphology of PrP(106–126) fibrils in the presence of enantiomeric Lys-C-dots. A–C) AFM images (recorded in wet conditions) of PrP(106–126) deposited upon a silicon wafer coated with a DMPC:DMPG lipid bilayer (1:1 mole ratio) A) in the absence of C-dots, B) in the presence of L-Lys-C-dots, and C) in the presence of D-Lys-C-dots. D–F) Cryo-TEM of PrP(106–126) in DMPC:DMPG vesicle solutions, D) in the absence of C-dots, E) in the presence of L-Lys-C-dots, and F) in the presence of D-Lys-C-dots. Bars correspond to 200 nm.

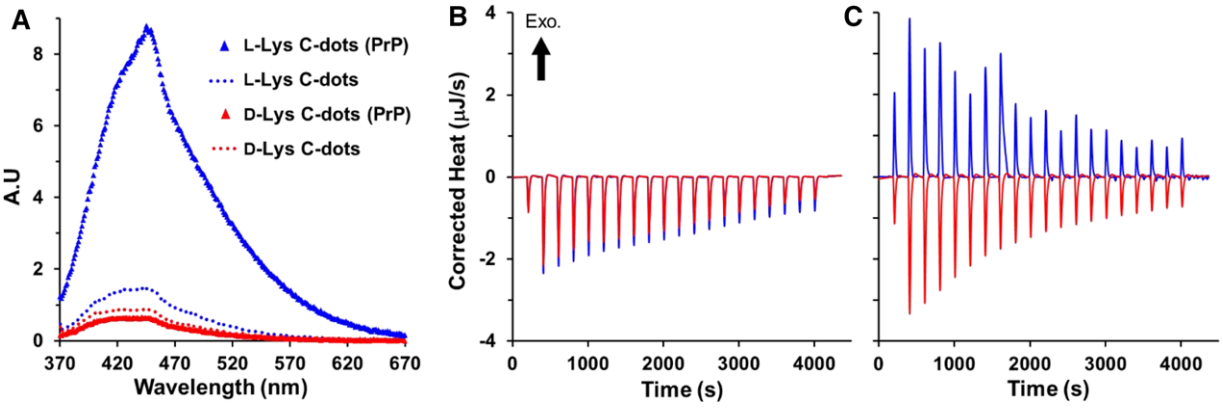

Figure 4. Interactions C-dots with PrP and lipid bilayers. A) Fluorescence emission spectra of the C-dots in presence of PrP ($n = 3$, each containing four replicates). B–C) Isothermal titration calorimetry patterns for: B) PrP(106–126) titrated into a solution of C-dots; C) DMPC:DMPG lipid vesicle solution titrated into a solution of C-dots. Experiments were repeated three times ($n = 3$).

the D-Lys-C-dot-treated sample compared to the native peptide. The AFM and cryo-TEM data in Figure 3 complement the ThT and CD experiments (Figure 2), confirming that the C-dots interfered with the fibril assembly process of PrP(106–126). In particular, the microscopy analyses provide vivid evidence for the chiral effect, that is, the much more pronounced effect of L-Lys-C-dots upon PrP(106–126), as compared to D-Lys-C-dots.

An important question one needs to address concerns the nature of interactions between the Lys-C-dots and PrP(106–126) and/or the lipid bilayers, and the implications for the aggregation process. ζ-potential measurements recorded for the two lysine-C-dots reveal that both particles exhibit similar, small negative surface charges ascribed to the carboxyl groups of the lysine (Figure S6, Supporting Information). This result indicates that electrostatic interactions of the Lys-C-dots are likely not the primary determinant in modulating the PrP(106–126) aggregation pathway. We further assessed the chiral interactions between the C-dots and PrP(106–126) and their molecular implications using fluorescence spectroscopy and isothermal titration calorimetry (ITC), Figure 4. Figure 4A depicts the fluorescence emission spectra (350 nm excitation) of the C-dots, and the effects of interactions with PrP(106–126). Although L-Lys-C-dots and D-Lys-C-dots alone exhibited similar emission spectra (Figure 4A, broken spectra), addition of PrP(106–126) led to a dramatic increase in the fluorescence emission spectrum of the L-Lys-C-dots (Figure 3A, blue triangles).

D-Lys-C-dots, on the other hand, did not experience an increase in fluorescence emission. The significantly different fluorescence spectra in Figure 4A indicate that L-Lys-C-dots interact differently with PrP(106–126) compared to D-Lys-C-dots, echoing the chiral discrimination data presented in Figures 2 and 3. The difference in fluorescence intensities may be a result of a more pronounced hydrophobic environment for the L-Lys-C-dots compared to the D-Lys-C-dots. This scenario may be due to "matching" of the C-dot and peptide chirality, promoting stronger interaction and closer proximity of the C-dots to the peptide aggregates, thereby shielding the C-dots from the aqueous environment.

The ITC results in Figure 4B,C provide further evidence for the significance of chiral interactions involving L-Lys-C-dots and D-Lys-C-dots, respectively, and point to C-dots' chiral interactions with the *lipid bilayer* as a prominent factor in modulation of PrP(106–126) fibrillation. In the ITC experiments depicted in Figure 4B, PrP(106–126) was titrated into solutions of the Lys-C-dot enantiomers and the reaction heats were measured (Figure 4B). In both enantiomeric Lys-C-dot samples, the interactions were endothermal throughout the titration and the corrected heat measurements did not differ significantly (although the isotherm of L-Lys-C-dots points to slightly more endothermal interactions with the peptide, Figure 4B). While this result indicates a similar enthalpy of interactions between PrP(106–126) and the two C-dot enantiomers, the ITC results obtained for C-dot interactions with the DMPC:DMPG vesicles portray a dramatic chiral effect (Figure 4C). Specifically, while the D-Lys-C-dots reacted *endothermally* with the DMPC:DMPG vesicles, the interaction of the vesicles with the L-Lys-C-dots was *exothermal*. This opposing calorimetric reaction pattern indicates that chirality played a major role in C-dot/bilayer interaction. Both DMPC and DMPG are synthetic L-enantiomeric phospholipids; accordingly, the exothermal nature of the interaction with L-Lys-C-dots may indicate greater thermodynamic stability.

3. Discussion

The experimental data in Figures 1–4 demonstrate clear chiral interference in membrane-induced structural transformations and aggregation of PrP(106–126). Indeed, the different spectroscopy and microscopy techniques applied complemented each other, illuminating the different facets of the chiral effects of L-Lys-C-dots and D-Lys-C-dots, respectively. Specifically, significant conformational changes of PrP(106–126) were induced by the two chiral C-dots during the aggregation process, reflected in the CD spectroscopy analysis (Figure 2B). In particular, inhibition of β-sheet formation by L-Lys-C-dots was clearly apparent. These data were consistent with the ThT kinetic measurements in Figure 2A, pointing to significant remodeling of PrP(106–126) aggregation in the presence of D-Lys-C-dots, and particularly L-Lys-C-dots.

In correlation to the ThT kinetic study, the microscopy analyses (Figure 3) attest to dramatic chiral effects upon the abundance and morphology of PrP(106–126) fibrils, induced by the Lys-C-dots, particularly L-Lys-C-dots. The AFM data, in particular, suggest that inhibition of PrP(106–126) fibrillation pathway has two facets—both reduction of overall fibril concentration, as well as significant fragmentation (or shortening) of the assembled fibrils. Both aspects, in fact, might be related to the disruption of initial β-sheet folding by the two C-dot species, apparent in the CD experiments outlined in Figure 2B.

The dramatic influence of lysine-C-dots on PrP(106–126) solution conformations and aggregation is not due to electrostatic interactions with the lysine moieties, as the results presented in Figures 2–4 clearly show chiral differences between the two C-dot enantiomers. Furthermore, while PrP(106–126) has three positively charged residues and is thought to interact with polar headgroups of membrane lipids, the Lys-C-dots charge is negligible. The ITC data in Figure 4 hint at the significance of chiral interactions between the lysine-C-dots, particularly L-Lys-C-dots, and lipid bilayers as an important factor modulating PrP(106–126) fibrillation in solution. Many studies have demonstrated that PrP aggregation intimately depends upon interactions of the peptide with lipid bilayers.[11,15,17,55] It is thus conceivable that the C-dots interfere with lipid interactions of PrP(106–126), thereby remodeling its fibrillation pathways. Indeed, since C-dot/bilayer interactions are chiral in nature (i.e., Figure 4C), the chiral effect should be manifested as well in the modulation of the membrane-mediated PrP(106–126) fibrillation.

A wide range of compounds have been examined as potential amyloid inhibitors. An effective inhibitor should be biocompatible, stable in physiological conditions, and not induce toxic effects by itself. C-dots exhibit attractive properties in that regard. C-dots are produced from diverse carbon-containing compounds, making possible tuning of their structural properties and biological compatibility. Moreover, their small dimensions enable efficient transport in body tissues and delivery to target destinations, potentially even across the blood–brain barrier. Unlike other therapeutic nanoparticle vehicles comprising inorganic constituents, C-dots are produced from natural carbonaceous building blocks, making them intrinsically biocompatible and less toxic.[41,56,57]

Figure 5 illustrates a proposed model accounting for the chiral inhibition of PrP(106–126), based upon the experimental data in Figures 1–4. In the control system (no C-dots added, Figure 5, top), the DMPC/DMPG bilayer induces formation of elongated PrP(106–126) fibrils. In contrast, L-Lys-C-dots significantly disrupt PrP(106–126) fibrillation both through direct interactions with the peptide, as well as docking onto the bilayer thus shielding it from interactions with the PrP(106–126) (Figure 5, middle). D-Lys-C-dots, on the other hand, also interfere with PrP(106–126) fibrillation albeit to a lesser extent (bottom route in Figure 5). The fibril modulation effect induced by D-Lys-C-dots is possibly related to their slight negatively charged surface, thereby disrupting membrane-induced aggregation of the peptide. The more pronounced inhibition of PrP(106–126) by L-Lys C-dots as compared to D-Lys-C-dots might be also related to the ability of the L-Lys C-dots to disrupt β-sheet folding of the monomer and concurrent oligomer formation. Indeed, Walsh et al.[58] have shown that PrP(106–126) is stabilized by van der Waals forces between the aliphatic residues (111–126) and electrostatic attraction between Lys 110 and the carboxylic termini (adjacent to residue 126), forming zipper-like parallel structure (Figure 5). According to the proposed model outlined in Figure 5, L-Lys C-dots might compete with Lys-100 interaction with the carboxyl termini, thereby weaken the β-sheet assembly.

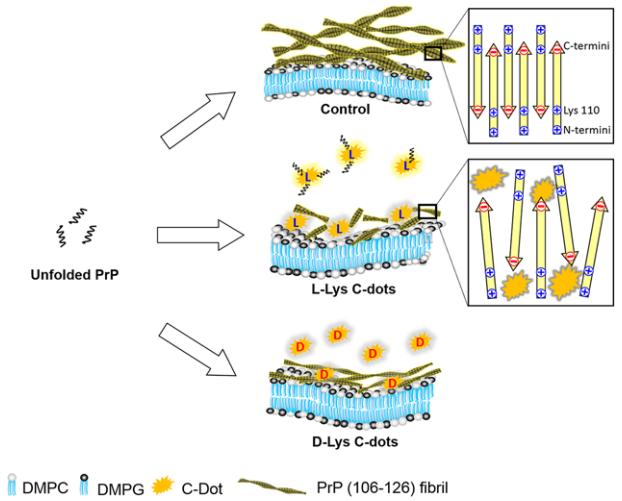

Figure 5. Proposed model accounting for chiral PrP fibril inhibition by Lys-C-dots. PrP(106–126) undergoes extensive fibrillation in the presence of a DMPC/DMPG lipid bilayer (top). L-Lys-C-dots inhibit fibrillation and remodel the fibrils due to chiral interactions with both the bilayer interface and the C-dots (middle). D-Lys-C-dots induce lesser effect although the fibrils adopt different morphologies compared to the control peptide (bottom).

4. Conclusions

This study demonstrates a remarkable chiral inhibition of the assembly and fibrillation of the amyloidogenic determinant of the prion protein, induced by Lys-C-dots in the presence of DMPC/DMPG vesicles. The experiments reveal that L-Lys-C-dots significantly modulated structural transformations of PrP(106–126) in vesicle solutions, yielding less abundant fibril aggregates exhibiting different morphologies (shorter, truncated fibrils) compared to the unperturbed peptide aggregating in vesicle solutions. D-Lys-C-dots, on the other hand, had lesser, albeit experimentally noticeable effect upon PrP(106–126) fibrillation. The data suggest that the chiral inhibition effects are due to both interference of the C-dots with membrane-induced peptide fibrillation pathways as well as direct interactions of the C-dots with the aggregating peptide. This work points to a new avenue towards development of chiral carbon nanomaterials as therapeutic substances against amyloid diseases.

5. Experimental Section

Materials: The amyloidogenic fragment of the prion protein, KTNMKHMAGAAAAGAVVGGLG (sequence 106–126; molecular wt. 1912.3), denoted PrP(106–126), was custom synthesized, purified by high performance liquid chromatography to 95% and supplied as a lyophilized powder by Peptron, Daejeon, South Korea. 1,2-dimyristoyl-sn-glycero-3-phosphocholine (DMPC) and 1,2-ditetradecanoyl-sn-glycero-3-phospho-(1′-rac-glycerol) (sodium salt) (DMPG) were purchased from Avanti Polar Lipids. 1,1,1,3,3,3-Hexafluoro-2-propanol (HFIP), thioflavin T (dye content > 65%), ethylene glycol, O,O′-bis(2-amino propyl), polypropylene glycol-block-polyethylene glycol-block-polypropyleneglycol1 were purchased from Sigma-Aldrich (Rehovot, Israel). D-Lysine and L-lysine (99% purity) were purchased from Tzamal D-Chem Laboratories (Petah-Tikva, Israel).

One-Pot Synthesis of Chiral Lysine-Modified C-dots: 400 mg D- or L-lysine were mixed with 10 mL of ethylene glycol and 100 µL of O,O′-bis(2-amino propyl)polypropyleneglycol-block-polyethylene-glycol-block-polypropyleneglycol1. The mixture was heated at ≈170 °C for 3 h to allow the C-dots to form. Thereafter, the solutions of the chiral C-dots were purified by dialysis in deionized water (18.2 MΩcm, Thermo Scientific).

Preparation of Lipid Vesicles: Vesicles consisting of DMPC:DMPG, 1:1 mole ratio, were prepared by dissolving the two lipid components in a chloroform/ethanol (1:1, v/v) mixture and drying the solution under vacuum. Small unilamellar vesicles (SUVs) were prepared from the dried lipid powder in deionized water by sonication, using Sonics Vibra-cell VCX-130 sonicator (Newtown, CT, USA) at room temperature for 10 min at 20% amplitude. Vesicle suspensions were allowed to anneal for 1 h at room temperature prior to being used.

Sample Preparation: PrP(106–126) was dissolved in HFIP at a concentration of 4 mM and stored at −20 °C until use. For each experiment, the solution was thawed, and the required amount was dried by evaporation for 4–5 h at a pressure of 40 mbar to remove the HFIP. The dried peptide sample was dissolved in deionized water at room temperature. Solutions of C-dots was added into the PrP(106–126) solutions at the required peptide concentrations (100 µM and 200 µM stock solutions).

ThT Fluorescence Kinetic Assay: The fluorescence of PrP samples (total volume of 100 µL, 50 µM PrP, 200 µM DMPC:DMPG lipid vesicle solution) in the absence or presence of 0.1 mg mL^{-1} Lys-C-dots was measured in 96-well path cell culture plates on Biotek Synergy H1 plate reader (Biotek, Winooski, VT, USA) at 25 °C. ThT aqueous solution was added to final concentration of 10 µM per well. Fluorescence was recorded every minute over 80 min at an excitation wavelength of 440 nm and an emission wavelength of 490 nm. The self-fluorescence of the C-dots was deducted from measured fluorescence for each sample.

CD Spectroscopy: CD spectra were recorded in the range of 190–260 nm on a Jasco J-715 spectropolarimeter (Tokyo, Japan) using a 0.01-cm quartz cuvette for C-dot samples at a concentration of 10 mg mL^{-1}, and a 0.1-cm quartz cuvette for the PrP(106–126) samples. Each spectrum was run six times and the averaged spectra are presented. Samples contained 100 µM PrP and DMPC:DMPG lipid vesicles (200 µM final lipid concentration) in the absence or presence of 0.2 mg mL^{-1} Lys C-dots.

Cryogenic Transmission Electron Microscopy: PrP(106–126) solutions were prepared as described above at concentration of 50 µM in presence or absence of Lys C-dots (0.1 mg mL^{-1}). After 60 min of incubation at room temperature for the preparation of the solution, a 3-µL droplet was deposited on a glow-discharged TEM grid (300 mesh Cu Lacey substrate grid; Ted Pella). The excess liquid was blotted with a filter paper and the specimen was rapidly plunged into liquid ethane precooled with liquid nitrogen in a controlled environment (Leica EM GP). The vitrified samples were transferred to a cryo-specimen holder and examined at −181 °C using a FEI Tecnai 12 G2 TWIN TEM operated at 120 kV in low-dose mode. The images were recorded with a Gatan charge-coupled device camera (model 794).

Atomic Force Microscopy: The lipid vesicle aqueous solution (80 µL, 1 mM DMPC:DMPG) was deposited on a silicon wafer and allowed to dry at 40. A 80-µL sample of a 50-µM solution of PrP (without or with 0.1 mg mL^{-1} C-dots) was placed on top of the lipid-coated surface and scanned by AFM under wet conditions (Cypher ES, Asylum Research, an Oxford Instruments company, Goleta, CA), in tapping mode. All images were acquired using a silicon probe (BL-AC40TS, Olympus) under the following conditions: spring constant 0.09 N m^{-1}, frequency 25–35 kHz, and a tip with radius 9 nm.

C-dot Fluorescence: C-dot fluorescence was measured at 25 °C in 96-well path cell culture plates on Biotek Synergy H1 plate reader (Biotek, Winooski, VT, USA). Each well contained a 100-µL sample of 50 µM PrP(106–126) and 200 µM DMPC:DMPG lipid vesicle solution in the absence or presence of 0.1 mg mL^{-1} Lys C-dots. Fluorescence emission spectra were recorded at an excitation wavelength of 350 nm in the range of 370–700 nm.

Isothermal Titration Calorimetry ITC: PrP was dried as described above and dissolved in Tris-buffered saline (TBS 0.01M, pH 7.4, 150 mM NaCl). Lipid vesicles (DMPC:DMPG, 0.6 mM final lipid concentration) were

prepared as described above and dissolved in TBS. Lys C-dots were diluted with TBS to final concentration of 0.1 mg mL^{-1}. A sample of 300 µL of the C-dots solution was inserted into the Nano ITC low volume cell (TA Instruments, Newcastle, DE). The titrating syringe was filled with 50 µL of 0.6 mM lipid vesicle solution, 100 mM PrP solution or pure TBS. After equilibrium had been reached, injection of 2.5 µL aliquots was carried out every 250 s for a total of 90 min.

Statistical Analysis: Thioflavin T kinetics were recorded four times, each containing three sample replicates. Data are presented as mean ± SD. Circular dichroism was measured four times for each sample and the spectra were normalized according to the sample concentration and cuvette length. Samples containing PrP were also normalized to the number of residues.

Supporting Information

Supporting Information is available from the Wiley Online Library or from the author.

Acknowledgements

The authors are grateful to Dr. Einat Nativ-Roth for cryo-TEM imaging.

Conflict of Interest

The authors declare no conflict of interest.

Keywords

amyloid diseases, amyloid inhibitors, carbon dots, chiral nanoparticles, prion protein

Received: January 24, 2018
Revised: April 15, 2018
Published online: May 28, 2018

[1] J. D. Sipe, M. D. Benson, J. N. Buxbaum, S.-I. Ikeda, G. Merlini, M. J. M. Saraiva, P. Westermark, *Amyloid* **2010**, *17*, 101.
[2] S. Feng, X. H. Song, C. M. Zeng, *FEBS Lett.* **2012**, *586*, 3951.
[3] S. Il Yoo, M. Yang, J. R. Brender, V. Subramanian, K. Sun, N. E. Joo, S. H. Jeong, A. Ramamoorthy, N. A. Kotov, *Angew. Chem. Int. Ed.* **2011**, *50*, 5110.
[4] J. P. Taylor, *Science* **2002**, *296*, 1991.
[5] F. Mohammadi, A. Mahmudian, M. Moeeni, L. Hassani, *RSC Adv.* **2016**, *6*, 23148.
[6] M.-B. Ebrahim-Habibi, M. Amininasab, A. Ebrahim-Habibi, M. Sabbaghian, M. Nemat-Gorgani, *Biopolymers* **2010**, *93*, 854.
[7] J.-K. Choi, I. Cali, K. Surewicz, Q. Kong, P. Gambetti, W. K. Surewicz, S. B. Prusiner, *Proc. Natl. Acad. Sci.* **2016**, *113*, 13851.
[8] A. Aguzzi, C. Sigurdson, M. Heikenwaelder, *Annu. Rev. Pathol.* **2008**, *3*, 11.
[9] N. J. Cobb, W. K. Surewicz, *Biochemistry* **2009**, *48*, 2574.
[10] S. B. Prusiner, *Proc. Natl. Acad. Sci. U. S. A.* **1998**, *95*, 13363.
[11] R. Malishev, S. Nandi, S. Kolusheva, S. Shaham-Niv, E. Gazit, R. Jelinek, *Biochim. Biophys. Acta Biomembr.* **2016**, *1858*, 2208.
[12] M. Waqas, H.-M. Lee, J. Kim, G. Telling, J.-K. Kim, D.-H. Kim, C. Ryou, *Mol. Cell Biochem.* **2017**, *428*, 57.
[13] P. E. Fraser, *J. Biol. Chem.* **2014**, *289*, 19839.
[14] K. A. B. Kellett, N. M. Hooper, *Prion* **2009**, *3*, 190.
[15] L. De Gioia, C. Selvaggini, E. Ghibaudi, L. Diomede, O. Bugiani, G. Forloni, F. Tagliavini, M. Salmona, *J. Biol. Chem.* **1994**, *269*, 7859.
[16] P. Walsh, G. Vanderlee, J. Yau, J. Campeau, V. L. Sim, C. M. Yip, S. Sharpe, *J. Biol. Chem.* **2014**, *289*, 10419.
[17] N. Gal, A. Morag, S. Kolusheva, R. Winter, M. Landau, R. Jelinek, *J. Am. Chem. Soc.* **2013**, *135*, 13582.
[18] G. P. Gorbenko, P. K. J. Kinnunen, *Chem. Phys. Lipids* **2006**, *141*, 72.
[19] C. Cecchi, M. Stefani, *Biophys. Chem.* **2013**, *182*, 30.
[20] B. Y. Feng, B. H. Toyama, H. Wille, D. W. Colby, S. R. Collins, B. C. H. May, S. B. Prusiner, J. Weissman, B. K. Shoichet, *Nat. Chem. Biol.* **2008**, *4*, 197.
[21] P. Alam, K. Siddiqi, S. K. Chturvedi, R. H. Khan, *Int. J. Biol. Macromol.* **2017**, *103*, 208.
[22] A. J. Doig, P. Derreumaux, A. Pastore, G. Wei, *Curr. Opin. Struct. Biol.* **2015**, *30*, 50.
[23] C. Soto, E. M. Sigurdsson, L. Morelli, R. Asok Kumar, E. M. Castaño, B. Frangione, *Nat. Med.* **1998**, *4*, 822.
[24] C. Ryou, W. B. Titlow, C. E. Mays, Y. Bae, S. Kim, *Biomaterials* **2011**, *32*, 3141.
[25] C. Cabaleiro-Lago, F. Quinlan-Pluck, I. Lynch, S. Lindman, A. M. Minogue, E. Thulin, D. M. Walsh, K. A. Dawson, S. Linse, *J. Am. Chem. Soc.* **2008**, *130*, 15437.
[26] N. Gao, H. Sun, K. Dong, J. Ren, X. Qu, *Chem. A Eur. J.* **2015**, 829.
[27] C. Soto, *Mol. Med. Today* **1999**, *5*, 343.
[28] R. Malishev, S. Nandi, S. Kolusheva, Y. Levi-Kalisman, F. G. Klärner, T. Schrader, G. Bitan, R. Jelinek, *ACS Chem. Neurosci.* **2015**, *6*, 1860.
[29] B. Cheng, H. Gong, H. Xiao, R. B. Petersen, L. Zheng, K. Huang, *Biochim. Biophys. Acta* **2013**, 4860.
[30] Y. Porat, A. Abramowitz, E. Gazit, *Chem. Biol. Drug Des.* **2006**, *67*, 27.
[31] N. Rubin, E. Perugia, M. Goldschmidt, M. Fridkin, L. Addadi, N. Rubin, E. Perugia, M. Goldschmidt, M. Fridkin, L. Addadi, *J. Am. Chem. Soc.* **2008**, *130*, 4602.
[32] N. Kokkoni, K. Stott, H. Amijee, J. M. Mason, A. J. Doig, *Biochemistry* **2006**, *32*, 9906.
[33] J. Kellock, G. Hopping, B. Caughey, V. Daggett, *J. Mol.* **2016**, *428*, 2317.
[34] V. Strauss, J. T. Margraf, C. Dolle, B. Butz, T. J. Nacken, J. Walter, W. Bauer, W. Peukert, E. Spiecker, T. Clark, D. M. Guldi, *J. Am. Chem. Soc.* **2014**, *136*, 17308.
[35] N. L. Teradal, R. Jelinek, *Adv. Healthc. Mater.* **2017**, *6*, 1.
[36] R. Jelinek, *Carbon Quantum Dots Synthesis, Properties and Applications*, Springer International Publishing, Switzerland, **2016**, 47.
[37] S. Zhu, Q. Meng, L. Wang, J. Zhang, Y. Song, H. Jin, K. Zhang, H. Sun, H. Wang, B. Yang, *Angew. Chem. Int. Ed.* **2013**, 3953.
[38] X. Sun, Y. Lei, *Trends Anal. Chem.* **2017**, *89*, 163.
[39] Z. Zhang, T. Zheng, X. Li, J. Xu, H. Zeng, *Part. Part. Syst. Charact.* **2016**, *33*, 457.
[40] S. N. Baker, G. A. Baker, *Angew. Chem. Int. Ed.* **2010**, *49*, 6726.
[41] C. Ding, A. Zhu, Y. Tian, *Acc. Chem. Res.* **2013**, *47*, 20.
[42] S.-J. Yu, M.-W. Kang, H.-C. Chang, K.-M. Chen, Y.-C. Yu, *J. Am. Chem. Soc.* **2005**, *127*, 17604.
[43] B. R. Selvi, D. Jagadeesan, B. S. Suma, G. Nagashankar, M. Arif, K. Balasubramanyam, M. Eswaramoorthy, T. K. Kundu, *Nano Lett.* **2008**, *8*, 3182.
[44] H. Li, X. He, Z. Kang, H. Huang, Y. Liu, J. Liu, S. Lian, C. Him, A. Tsang, X. Yang, S.-T. Lee, *Angew. Chem. Int. Ed.* **2010**, *49*, 4430.
[45] J. Peng, W. Gao, B. K. Gupta, Z. Liu, R. Romero-Aburto, L. Ge, L. Song, L. B. Alemany, X. Zhan, G. Gao, S. A. Vithayathil, B. A. Kaipparettu, A. A. Marti, T. Hayashi, J.-J. Zhu, P. M. Ajayan, *Nano Lett.* **2012**, *12*, 844.
[46] S. K. Bhunia, L. Zeiri, J. Manna, S. Nandi, R. Jelinek, *ACS Appl. Mater. Interfaces* **2016**, *8*, 25637.
[47] S. K. Bhunia, A. Saha, A. R. Maity, S. C. Ray, N. R. Jana, *Sci. Rep.* **2012**, *3*, 1.

[48] G. Liu, M. R. Garrett, P. Men, X. Zhu, G. Perry, M. A. Smith, *Biochim. Biophys. Acta* **2005**, *3*, 246.
[49] X. Han, Z. Jing, W. Wu, B. Zou, Z. Peng, P. Ren, A. Wikramanayake, Z. Lu, R. M. Leblanc, *Nanoscale* **2017**, *9*, 12862.
[50] N. Suzuki, Y. Wang, P. Elvati, Z.-B. Qu, K. Kim, S. Jiang, E. Baumeister, J. Lee, B. Yeom, J. H. Bahng, J. Lee, A. Violi, N. A. Kotov, *ACS Nano.* **2016**, *10*, 1744.
[51] S. K. Bhunia, A. R. Maity, S. Nandi, D. Stepensky, R. Jelinek, *Chem. Bio. Chem.* **2016**, *17*, 614.
[52] S. Dolai, S. K. Bhunia, L. Zeiri, O. Paz-Tal, R. Jelinek, *ACS Omega* **2017**, *2*, 9288.
[53] Y. Zhang, L. Hu, Y. Sun, C. Zhu, R. Li, N. Liu, H. Huang, Y. Liu, C. Huang, Z. Kang, *RSC Adv.* **2016**, *6*, 59956.
[54] N. Massad-Ivanir, S. Kumar Bhunia, N. Raz, E. Segal, R. Jelinek, *NPG Asia Mater.* **2018**, *1*, e463.
[55] S. A. Kotler, P. Walsh, J. R. Brender, A. Ramamoorthy, *Chem. Soc. Rev.* **2014**, *43*, 6692.
[56] L. Wang, S. Zhu, T. Lu, G. Zhang, J. Xu, Y. Song, Y. Li, L. Wang, B. Yang, F. Li, *J. Mater. Chem. B* **2016**, *4*, 4913.
[57] Z. Qian, J. Ma, X. Shan, H. Feng, L. Shao, J. Chen, *Chem. A Eur. J.* **2014**, *20*, 2254.
[58] P. Walsh, K. Simonetti, S. Sharpe, *Structure* **2009**, *17*, 417.

